Remote Sensing of Environment 232 (2019) 111338

Contents lists available at ScienceDirect

Remote Sensing of Environment

journal homepage: www.elsevier.com/locate/rse

Remote sensing monitoring of multi-scale watersheds impermeability for urban hydrological evaluation

Zhenfeng Shao[a], Huyan Fu[a,*], Deren Li[a], Orhan Altan[b], Tao Cheng[a]

[a] State Key Laboratory for Information Engineering in Surveying, Mapping and Remote Sensing, Wuhan University, Wuhan 430079, China
[b] Department of Geomatics Engineering, Istanbul Technical University, Turkey

ARTICLE INFO

Edited by: Jing M. Chen

Keywords:
Impervious surfaces
Urban hydrological environment
Google earth engine
Multi-scale
Watersheds

ABSTRACT

Urban impervious surface coverage is an important parameter to understand effects of hydro-environment on the process of urbanization. Impervious surfaces have altered urban hydrological process, spatial and temporal distribution of water resources and water environment quality and led to increasing frequency and intensity of urban waterlogging. In view of the impact of the increase of impervious surface on urban hydrological environment, there are two problems in current research and application: (1) urban hydrological modeling and impermeability ratio are computed according to multi-level administrative units rather than watersheds; (2) the entire urban hydrological environment is an organic whole, but the urban watersheds system within a city have not been monitored dynamically by considering adjacent watersheds. In view of these two problems, the main innovative points in this research work include (1) first, urban multi-scale watersheds are defined, and impermeability ratios are calculated at multi-scale watersheds level for urban hydrological modeling. (2) Based on urban DEM analysis, considering the interconnection of multiple urban water systems by calculating the dynamic impermeability ratios, the dynamic impact of urban rainfall and runoff changes on the whole urban hydrological environment is monitored. The results show overall impervious surface ratio of each watershed is proportional to the runoff. The ratio of the impervious surface reaches 20%, and the discharge is more than twice that when impervious ratio is 4%. It can be concluded that at watershed level a higher the degree of urbanization can lead to a larger change in the total run off, and the earlier shift of the peak flow.

1. Introduction

Urban expansion, evidenced by the growth of impervious surface areas (ISA) (e.g. building rooftops, pavements, parking lots and roads) (Kuang et al., 2013; Liu et al., 2014) is accompanied by the decrease of the natural lands (e.g. farmland, forest land, and water body). Impervious surfaces raise the duration, intensity, and velocity of surface runoffs, decrease the groundwater recharge and base flow, and increase the flood peak frequency and volume (Brun and Band, 2000; Moscrip and Montgomery, 1997). Urban impervious surface changes surface albedo, specific emissivity and surface roughness by modifying the structure of urban surface.

In recent years, urban flooding has become a global concern in many cities all over the world (Miller and Hess, 2017; Roodsari and Chandler, 2017; Sunde et al., 2016; Yao et al., 2016) because of its major negative impacts on public health, economic development, and quality of life especially in developing countries such as China, India, Bangladesh, Nepal(Ding et al., 2018; Wang et al., 2017; Xue et al., 2016). Traditional solution to urban storm water is to build a gray drainage system and increase drainage networks and diameters of rainfall drains to rapidly drain the storm water away and then to store it at downstream facilities (Cembrano et al., 2004) (USEPA, 2000). However, the fast discharge of rainwater would cause a huge burden to the drainage system, causing urban flooding, river erosion, increasing suspended solids, and heavy metals pollution (Kong et al., 2017; Mei et al., 2018; Rosenberg et al., 2010).

A number of measures have been developed to manage urban storm water, such as water-sensitive urban design (WSUD) in Australia, and best management practices (BMPs) and Low Impact Development (LID) in the USA (USEPA,2000), sustainable drainage systems (SuDS) in the UK, urban design and development (LIUDD) in New Zealand. LID aims to mimic the pre-development hydrologic conditions and achieves hydrologic neutrality thus promoting storage, infiltration and evapotranspiration processes. Holman-Dodds et al. (2003) showed that by

* Corresponding author.
E-mail addresses: shaozhenfeng@whu.edu.cn (Z. Shao), fuhuyan@whu.edu.cn (H. Fu), drli@whu.edu.cn (D. Li), oaltan@itu.edu.t (O. Altan), taocheng@whu.edu.cn (T. Cheng).

https://doi.org/10.1016/j.rse.2019.111338
Received 31 October 2018; Received in revised form 15 July 2019; Accepted 18 July 2019

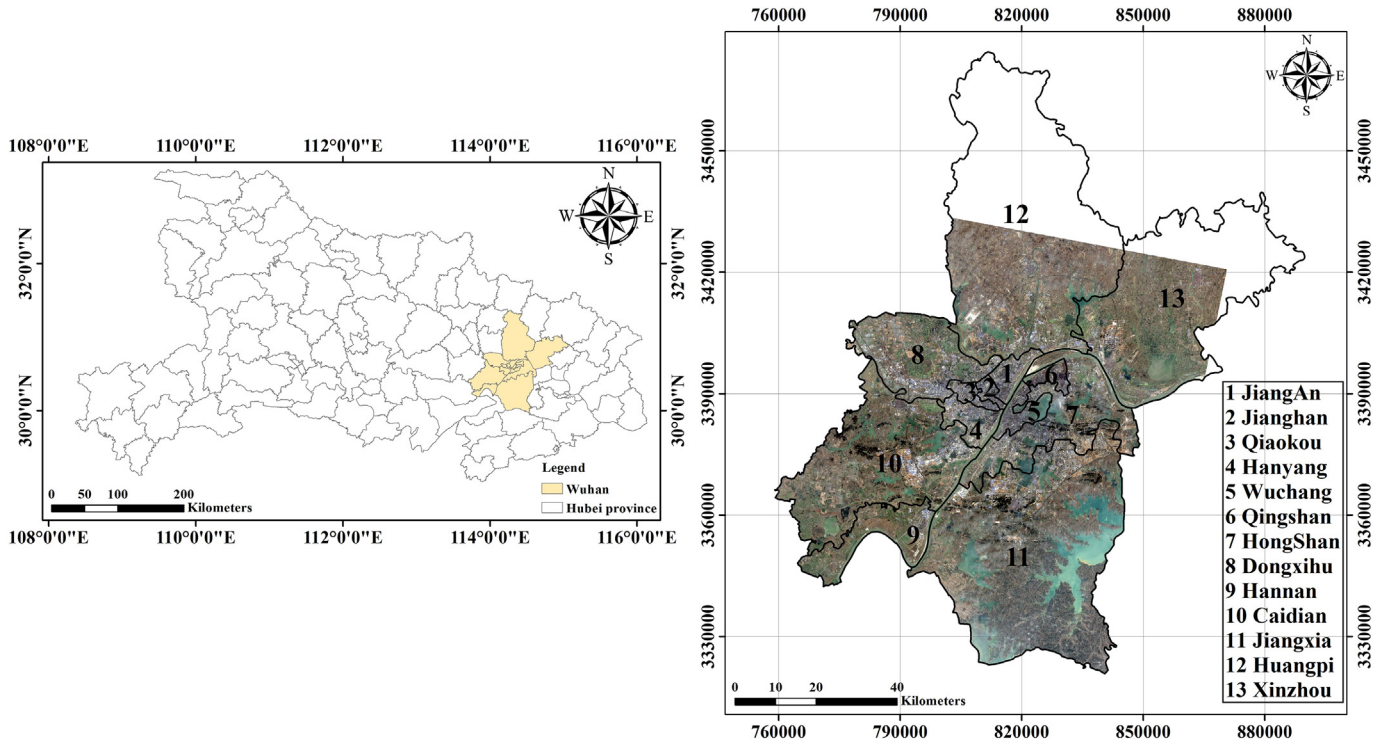

Fig. 1. The geographic location of the study area, Wuhan, China.

manipulating the layout of urbanized landscapes, it is possible to reduce impacts of impervious surfaces on hydrology relative to traditional, fully connected storm water systems. However, the amount of reduction was observed for both rainfall event size and soil texture, with greatest reductions being possible for small, relatively frequent rainfall events and more pervious soil textures. Palla and Gnecco (2015) selected green roofs and permeable pavements as source control systems to be applied to rooftops and parking lot areas respectively to reduce the impact of imperviousness at the catchment scale. Hu et al. (2017) assessed the performance of LID practices for mitigating flood inundation hazards as retrofitting technologies in an urbanized watershed in Nanjing, China. Kong et al. (2017) explored the hydrological responses of stormwater runoff characteristics to four different land use conversion scenarios under multiple LID implementations at the city scale using GIS-based Stormwater Management Model (SWMM). Jun and Fuling (2000) forecasted and analyzed urban waterlog-draining using decision support system based on the 4D data fusion technique.

To solve the urban waterlogging issue, the construction of sponge cities was proposed in china following the LID principles (Xu et al., 2018). The Sponge City, a new concept of urban water management, refers to the city with good flexibility to adapt to environmental change and to respond to natural disasters caused by rain (Chan et al., 2018; Li et al., 2018; Liu et al., 2017; Shao et al., 2016) However, studies of LID scenarios to date have been limited to the lot or block scale. Urban planning and urban management usually use the political boundaries, and the planning and reconstruction of Sponge Cities are also based on the administrative boundaries. However, urban water cycle, and surface runoff do not follow administrative boundaries.

Given the increased impact of impervious surface on urban hydrological environment, there are two problems in current research and application: (1) Within a city, the current research and application are based on multi-level administrative units such as city-administrative region (county) - street-community as a simulation analysis or statistical analysis unit, but not on the internal water system of the city to study the urban hydrological model. If the impermeability rate is counted according to multi-level administrative units rather than Watersheds, it cannot reflect the real characteristics of hydrological changes within the city; (2) the current planning of sponge city does not consider the specific urban water system that the city belongs to, nor does the entire urban hydrological environment as a whole be analyzed and modeled.

The statistical unit of impermeability in sponge city planning should be based on the watershed or multi-scale watersheds. Using administrative divisions to calculate imperviousness is only of mathematical significance and does not have physical and ecological value. For example, the water surface area of Wuhan City accounts for one quarter of the total area of the built-up area. If only the entire impervious rate of the built-up area is considered, the problem of high impermeability of land cannot be reflected. Current sponge city pilot area, considering the size of funds and renovation projects, usually chooses the pilot area according to the needs of urban construction and administrative divisions. The pilot zone uses the impermeability of the Pilot area for modeling and analysis. Because it is neither a complete water system nor a part of a certain water system (spanning multiple water systems), its urban hydrological effects of planning and modeling are difficult to achieve as scientifically considered as a full water system. This paper emphasizes the impervious rate of multi-scale watersheds, and takes them as the inputs to urban hydrological modeling. Therefore, in this study, we proposed a multi-level watersheds runoff monitoring model based on the analysis of urban impervious surfaces dynamics from 1987 to 2017 every five years. We aimed to explore the change of impervious surfaces in Wuhan during the past 30 years and analyze the relationship between impervious surfaces and urban surface runoff in four steps: (1) extracting the impervious surfaces using random forest from 1987 to 2017 from Landsat images with Google Earth Engine (GEE); (2) analyzing the spatiotemporal dynamics of impervious surfaces over the whole study period; (3) calculating the annual runoffs from 1987 to 2017 using the INFORWORKS model; and (4) exploring the relationship between impervious surfaces and urban waterlogging. The objective of this paper is to explore impervious surface ratios of multi-scale watersheds as indicators to help decision-makers understand the interactions between urban impervious surfaces distribution and runoff.

Table 1
Waterlogging area in typical year in Wuhan city.

Year	Maximum daily rainfall (mm)	Waterlogging situation
2011	200.5	Heavy rain on June 18, 88 serious waterlogging spots in central Wuhan City, traffic system paralyzed
2013	321	22 main roads and 75 communities were flooded, 250 thousand people suffered
2016	246.4	162 waterlogging spots, 206 waterlogging roads, and serious water in subway stations

2. Study area and data processing

2.1. Study area

The study area, Wuhan, is situated at the eastern Jianghan Plain in the middle part of China (113°41′E to 115°05′ E and 29°58′N to 31°22′ N) on the middle reaches of the Yangtze River at the intersection of the Yangtze and Han rivers (see Fig. 1). The city covers an area of 8494 km^2 with a population of 10.02 million. Wuhan has experienced rapid urban expansion in the past three decades.

According to the statistics of Wuhan Central Meteorological Observatory from 1951 to 2012, the annual rainfall in Wuhan has fluctuated between 700 and 2100 mm in the past 50 years (http://hb.cma.gov.cn/). During this period, there were 15 rainy years ($P \leq 25\%$) with an average precipitation of 1660.6 mm, 32 plain years ($25\% < P < 75\%$) with the average precipitation of 1218.7 mm, and 15 drought years ($P \geq 75\%$) with an average precipitation of 935.3 mm. In the past 10 years, rainstorm in Wuhan occurred in 2011, 2013 and 2016 (http://hb.cma.gov.cn/) (Table 1).

Wuhan is among the first for sponge cities in China. During the three-year pilot period from 2015 to 2017, Qingshan and Sixin in Hanyang, all parts of the city of Wuhan, was built with a total area of 38.5 km^2. The project includes seven aspects including residential areas, public buildings, parks and green spaces, urban roads, drainage pumping stations, urban water ecological restoration, and evaluation platform construction. The specific goal is to vigorously upgrade the urban rainwater management capacity to achieve annual runoff total control rate of over 70% in Qingshan demonstration zone, and over 80% in Sixin of Hanyang demonstration zone.

2.2. Data processing

The study area is located across three Landsat scenes (Path: 123, Row: 39; Path: 123, Row: 38; Path: 122, Row: 39). In this study, only the main tile (Path: 123, Row: 39) was selected to extract impervious surfaces and calculate urban runoffs. A total of 18 Landsat images (6 Landsat-5, 9 Landsat-7, and 3 Landsat-8) from 1987 to 2017 were requested through GEE in this study. The selected Landsat images were acquired in either December or November (Table 2). The clouds were removed for year 2012 Landsat images. As the scan-line corrector (SLC) of the Landsat 7 ETM+ sensor failed in 2003, the locations of SLC-off data were identified using band-specific gap mask files in each SLC-off data product. The vector data of Watersheds are provided by the Wuhan Water Affairs Bureau (see Table 3). Hourly and 5 minutes-interval precipitation data on July 7, 2013 were used from Hubei Meteorological Service. The DEM (Digital Elevation Model, DEM) data with 30 m resolution and the lakes boundary are obtained by Wuhan Natural Resources and Planning Bureau.

Table 2
The image data used in this study.

Sensor	Date
Landsat 5 TM	1987-12-31,1992-11-10,1997-11-08
Landsat 7 ETM+	2002-12-16, 2007-12-30, 2012-12-11
Landsat 8 OLI/TIRS	2017-12-17

3. Method

In this paper, watershed is defined as an evaluation unit of urban hydrological environment. The watershed is a catchment unit, providing the theoretical and technique foundation for calculating the runoff. The watershed has a multi-scale attribute, and finally constitutes the whole city water circulating system. Based on this evaluation unit, we define the impervious ratio of watershed and that of the whole water circulating system.

$$ISA\ ratio_{watershed} = ISA\ area_{watershed} / Area_{\text{inland surface of } watershed} \quad (1)$$

$$ISA\ ratio_{\text{basin network}} = ISA\ area_{\text{basin network}} / Area_{\text{inland surface of basin network}} \quad (2)$$

where $ISA\ ratio_{watershed}$ is the impervious ratio of watershed, $ISA\ ratio_{watershed}$ is the area of impermeable surface in watershed, $Area_{\text{inland surface of } watershed}$ is the inland area in watershed, and $Area_{water\ of\ watershed}$ is the area of water. $ISA\ ratio_{\text{basin network}}$ is the impervious ratio of basin network, $ISA\ area_{\text{basin network}}$ is the area of impermeable surface in the hydrographic system, $Area_{\text{inland surface of basin network}}$ is the inland surface area of the hydrographic system.

In this study, remote sensing monitoring of multi-scale watersheds impermeability for urban hydrological evaluation is realized. A multi-scale monitoring model on urban impervious surface watersheds was put forward. Fig. 2 presents the overall workflow of the procedures. Firstly, we employed data service based on the GEE platform; Landsat data from 1987 to 2017 were used for feature extraction and the VHR images from Google Earth were used as training and validation data, then RF classifier was used to extract urban impervious surface (Section 3.1). Secondly, multi-level watersheds were built and divided watersheds into four levels, cell watersheds, administration watersheds, dynamic watersheds, and city watershed, then relationship between the impervious surfaces and urban runoffs were analyzed for better understanding the urban eco-environment, especially for the prevention and control of urban waterlogging. Finally, the continuous runoff process at different urbanization degrees under the same precipitation event were simulated by hourly and 5 minutes-interval precipitation data on July 7, 2013.

3.1. Mapping impervious surface using GEE

Studies of impervious surfaces began in the field of urban hydrology in the 1970s (Brabec et al., 2002). At that time, extraction of land use types (including impervious surfaces) from medium/high spatial resolution remote sensing images mainly relied on field surveys or visual interpretation of high resolution aerial images (Goetz et al., 2003; Zhang et al., 2013). To meet the requirements of urban applications, remote sensing images have been widely utilized to extract urban ISA using different methods (Deng et al., 2017; Deng and Wu, 2013a, 2013b; Du et al., 2014; Im et al., 2012; Lu et al., 2011; Lu and Weng, 2006; Wu and Murray, 2003; Xian and Homer, 2010; Zhang et al., 2014, 2017, 2018; Zhuo et al., 2018). GEE is a cloud-based platform for scientific analysis and visualization of petabyte-scale geospatial datasets. It is set up for scientific analysis-ready data with a high performance by providing historical satellite images over decades (Chen et al., 2017; Dong et al., 2016; Gorelick et al., 2017; Huang et al., 2017; Johansen et al., 2015; Lee et al., 2016; Liu et al., 2018; Patela et al., 2015; Xiong et al., 2017).

Table 3
Twenty-two Watersheds in Wuhan.

Number	Watershed name	Number	Watershed name	Number	Watershed name
1	Beihu	8	Gongyegang	15	Huangxiaohe
2	Caidiandonghu	9	Guanlianhu	16	Jinyintan
3	Changqing	10	Hankou yanhe	17	Lannihu
4	Chenjiaji	11	Hankou yanjiang	18	Liangzihu
5	Chuanjiangchi	12	Hanyangyanhe	19	Qingshanzhen
6	Dongshahu	13	Hanyang yanjiang	20	Tangxunhu
7	Gangxi	14	Hexi	21	Tongshunhe
				22	Wuchang linjiang

Random Forest algorithm (Breiman, 2001, 1996) as a classifier, well-known for its superior performance on multi-dimensional features, was selected to extract the impervious surfaces from 1987 to 2017 in Wuhan. Six land cover types were identified: bright impervious surfaces, dark impervious surfaces, vegetation, high reflectance of bare land, low reflectance of bare land, and water bodies. For each type, the number of the samples was randomly selected by visual interpretation of the high spatial resolution Google Earth images and distributed evenly over the study area. Then the six land cover types were further categorized into three types, impervious surfaces (IS, including bright impervious surfaces and dark impervious surfaces), non-impervious surfaces (NIS, including vegetation, high reflectance of bare land and low reflectance of bare land), and water bodies (WB).

Normalized difference vegetation index (NDVI) (Crippen, 1990; Rouse et al., 1973), normalized difference water index (NDWI) (McFeeters, 1996), Normalized Difference Built Index (NDBI) (Zha et al., 2003), soil-adjusted vegetation index (SAVI) (Huete, 1988), and biophysical composition index (BCI) (Deng and Wu, 2012) were extracted as additional spectral features for classification.

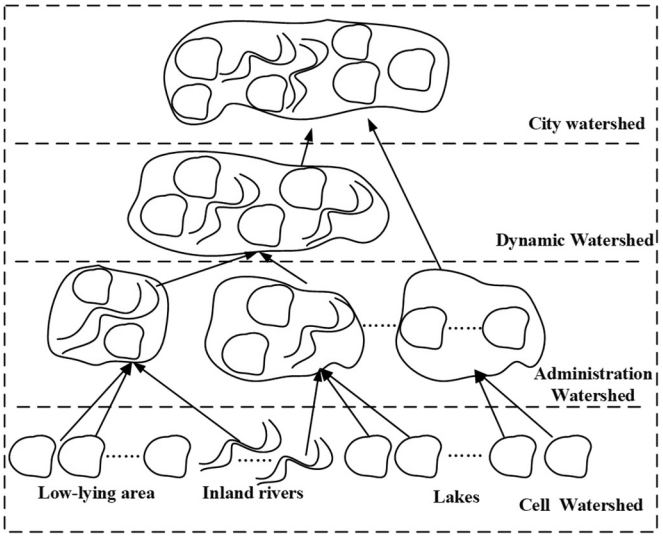

Fig. 3. City multi-level watersheds runoff monitoring model.

3.2. Urban multi-level watersheds runoff monitoring model

In this section, an urban multi-level watersheds runoff monitoring model was put forward. The model is to explore and define the unit of urban runoff monitoring. This unit is analyzed in relation with land use, urban management, urban hydrology, urban planning, urban design, and other related perspectives. The authors seek the unit of urban runoff monitoring from the hydrological cycle, which begins with

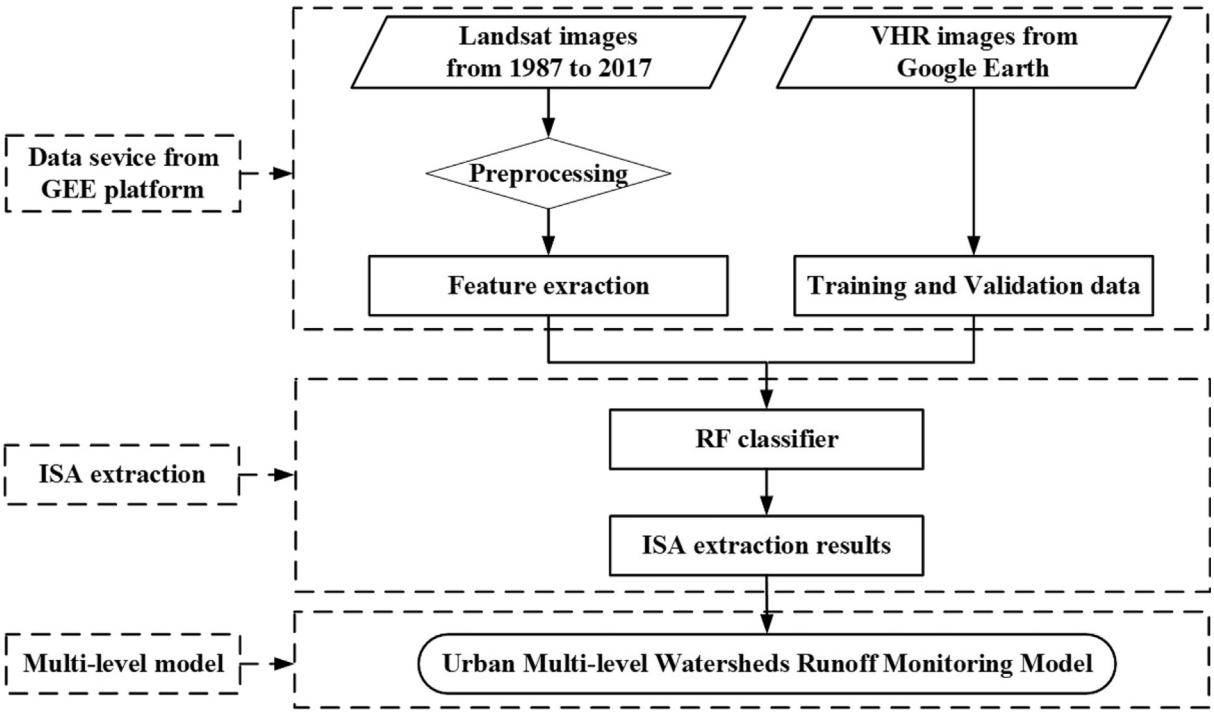

Fig. 2. The flowchart on remote sensing monitoring of multi-scale watersheds impermeability for urban hydrological evaluation using Google Earth Engine.

precipitation. The traditional precipitation is rainfall. Part of the rainfall will be transformed into evaporation by vegetation. The excess rainfall is divided into infiltration, overland runoff, and depression storage such as lakes, inland rivers.

The urban multi-level watersheds runoff monitoring model is constructed as follows (see Fig. 3):

(1) The basic level is the cell watershed. The cell watersheds consist of inland rivers, and lakes, which can be extracted from remote sensing images. In this paper, we assume that the low-lying areas, as candidate waterlogging points, belong to the cell watersheds, which can be detected from either DEM data or LiDAR-data.
(2) The second level is the urban hydrographic net, which can be selected as the administrative watershed. The concept of administrative watershed comes from the field of urban hydrology, which considers the total amount of confluence, the drainage capacity of pumping stations, and the drainage capacity of underground pipe networks. An administrative watershed usually includes several cell watersheds. In urban areas, alterations of the landscape form by urbanization result in increased runoff volumes. Consequently, urban areas are more susceptible to flooding than rural areas at an administrative watershed. The administrative watershed is strongly recommended to be used as a unit for monitoring urban water cycle and hydrological environment.
(3) The third level is the dynamic watershed for runoff monitoring. In an administrative watershed, after the drainage reaches the upper limit of the pipe networks and permeability of the pervious area, the water level in the administrative watershed will rise, and multiple cell watersheds may be linked together to become a bigger watershed. When the total amount of confluence is higher than the administrative watershed capacity, this administrative watershed will connect with the neighboring administrative watershed, and a much bigger watershed will form. We call this process a dynamic watershed. Dynamic watershed is very important to understand urban flood prevention, drainage and monitoring.
(4) The last level is the whole city watershed. As urban area has affiliations to a large basin at regional scale, this level of watershed monitoring considers the upstream catchment and the flow to downstream, which provide fundamental parameters for water resources assessment, development, and management of the whole city.

The multi-scale Watersheds defined in this paper contain the following meanings:

(1) The existing natural waters in cities belong to natural watersheds. For example, > 100 lakes and 2 rivers in Wuhan exist. Each river or lake is a natural cell watershed.
(2) Each waterlogging area can be regarded as a cell watershed during rainfall. For example, there are > 162 waterlogging areas in recent years in Wuhan. Each waterlogging area can be regarded as a cell watershed.
(3) Instead of using administrative boundaries, the proposed multi-level watershed runoff monitoring model should be used to reduce impervious surfaces in the city, and hence lower the risk of flooding.
(4) As the water level changes, different watersheds may merge into a new larger watershed at a given precipitation level.

3.3. Runoff volumes calculation

In this paper, the classical INFOWORKS model is chosen to calculate runoff volumes according to the perviousness-imperviousness ratios. The runoff model with constant rations is applied to the impervious surface catchment area, where the runoff can be accurately estimated. The Horton model (Horton, 1933) is adopted for the pervious surface.

Table 4
Parameters of runoff volume model.

Land cover	D(m)	Horton model			Fixed percentage runoff model
		f_0(mm/hr)	f_c(mm/hr)	k($1/hr$)	Fixed runoff coefficient
VE	0.008	125	6.3	2	
BL	0.008	78	6.3	2	
IS	0.002				0.95

The runoff volume model is shown in Eqs. (3)–(5) (see Table 4):

For impervious surface area:

$$R = c(P - D - E) \tag{3}$$

where R is the runoff volume, c is the constant runoff coefficient, P is the precipitation, D is the initial loss (mm), and E is the evaporation (mm).

While for pervious surface area:

$$R = (i - f)t - D - E \tag{4}$$

$$f = f_c + (f_0 - f_c)e^{-kt} \tag{5}$$

where i is the rainfall intensity (mm/hr), f is the infiltration intensity (mm/hr), P is the precipitation, D is the initial loss (mm), and E is the evaporation (mm), f_0 is the initial infiltration rate (mm/hr), f_c is the final (limiting) infiltration rate (mm/hr), k is the coefficient of the exponential term ($1/hr$), and t is the time (hr). The parameters in the runoff volume model are empirical values, which are derived from local water administrative departments, as follows:

The increase of impervious surface will lead to the acceleration of confluence process and the increase of hydrological active areas and frequency of larger peak discharge. The expected results of these changes include decreased lag times, increased storm flow volumes, and increased peak flows. The shape of hydrological curve has changed significantly. Fig. 4 is a typical precipitation event, the natural state (pre-urbanization), LID, BMPs, the flow process after urbanization (post-urbanization). Sponge city is the product of development of modern water ecology concepts such as LID and BMPs and the integration of traditional Chinese water governance wisdom.

4. Results

4.1. Accuracy assessment and dynamic analysis of impervious surface

The mapping results of impervious surface from 1987 to 2017 are

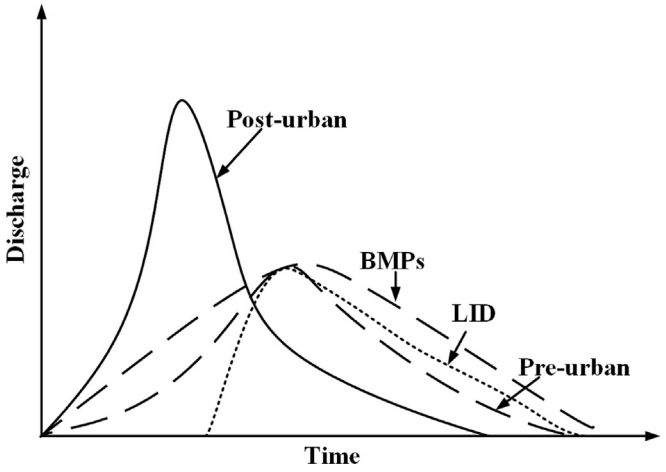

Fig. 4. Conceptual changes in hydrograph following urbanization (modified from Leopold, 1968).

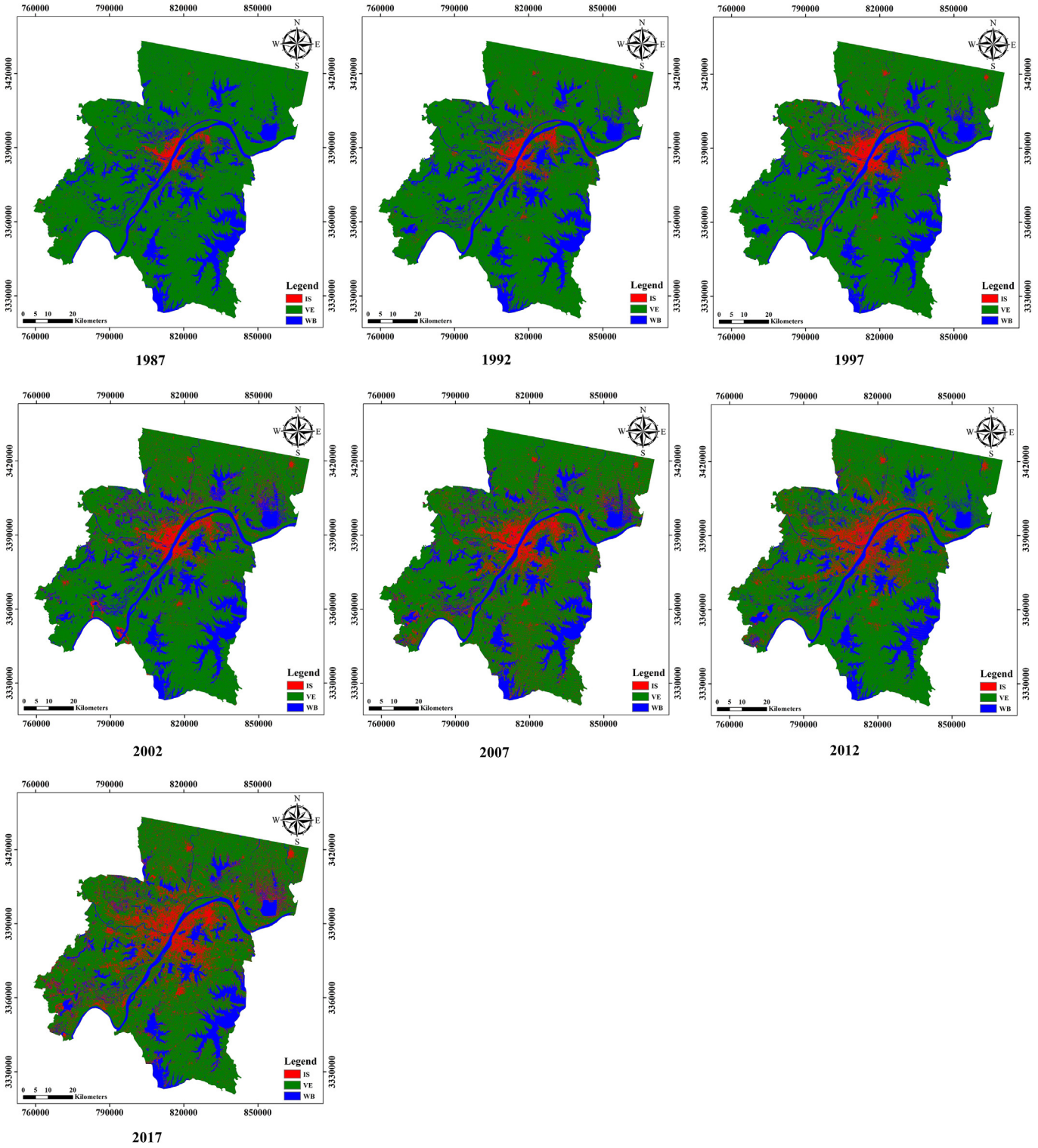

Fig. 5. ISA maps from 1987 to 2017 using GEE.

shown in Fig. 5. Confusions were observed between impervious surfaces and bare lands, which is mainly because of their similar spectral signatures.

Table 5 shows the total area of impervious surfaces in the study area from 1987 to 2017. From 1987 to 2017, ISA increased from 237.28 km^2 in 1987 to 1167.63 km^2 in 2017(Table 5). Firstly, ISA increased from 237.28 km^2 in 1987 to 663.81 km^2 in 2002.

Then, the impervious surface area and the ratio was in a steady state, from 663.81 km^2 in 2002 to 692.38 km^2 in 2007. The second rapid urban growth occurred from 2007 to 2017. Impervious surface areas increased from 692.38 km^2 in 2007 to 1167.63 km^2 in 2017.

4.2. The relationship between ISA and urban runoff at multi-scale watersheds

4.2.1. City level

Taking the city as a whole for calculation, the impervious surface ratio and the total surface runoff in Wuhan can be calculated as shown

Table 5
The relationship between ISA and urban runoffs in the whole city level.

	1987	1992	1997	2002	2007	2012	2017
IS (km^2)	237.28	423.36	530.27	663.81	692.38	790.18	1167.63
NIS (km^2)	5411.37	5221.55	5102.24	4869.5	4959.22	4897.09	4582
WB (km^2)	1240.53	1244.26	1256.66	1355.86	1235.41	1201.9	1139.54

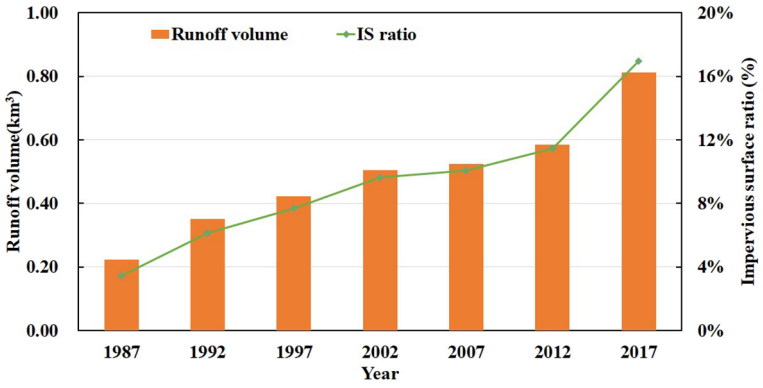

Fig. 6. Impervious surface ratios and runoff volume from 1987 to 2017 in Wuhan.

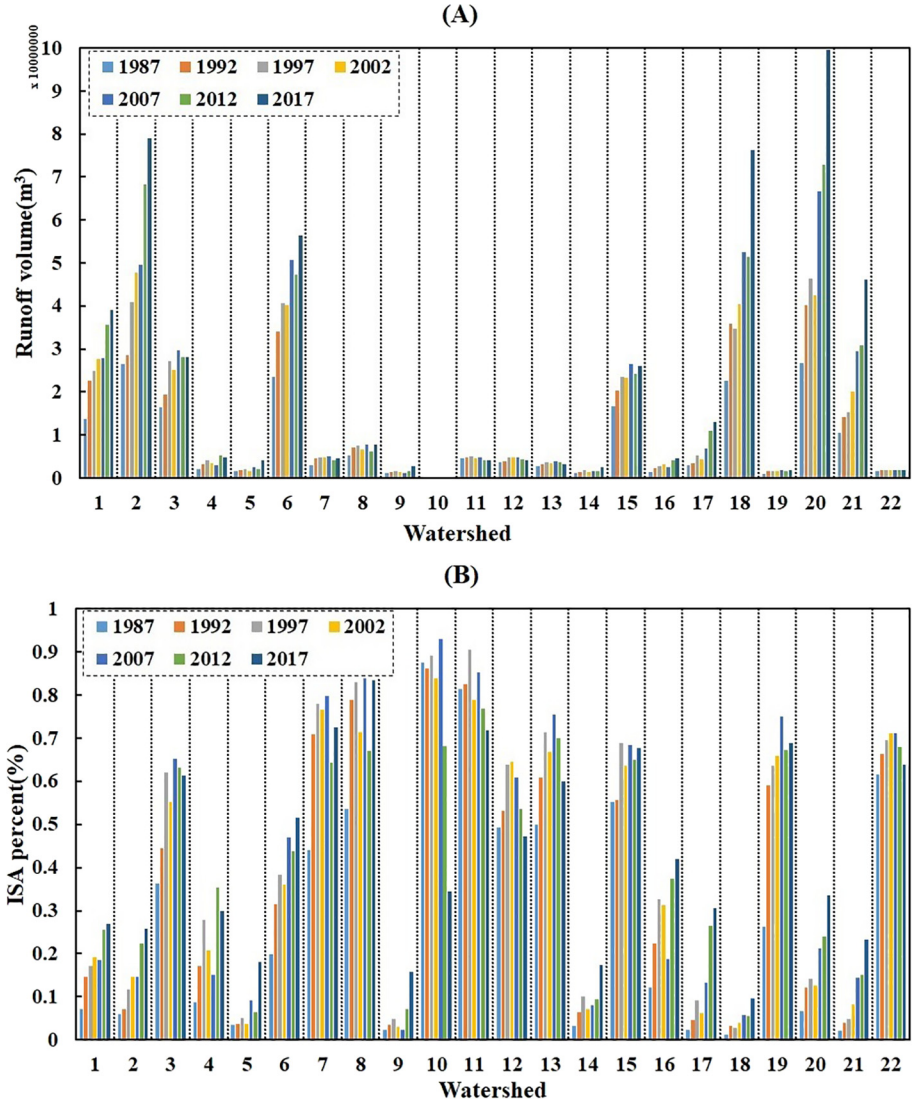

Fig. 7. The land cover area and urban runoff volume at watershed level.

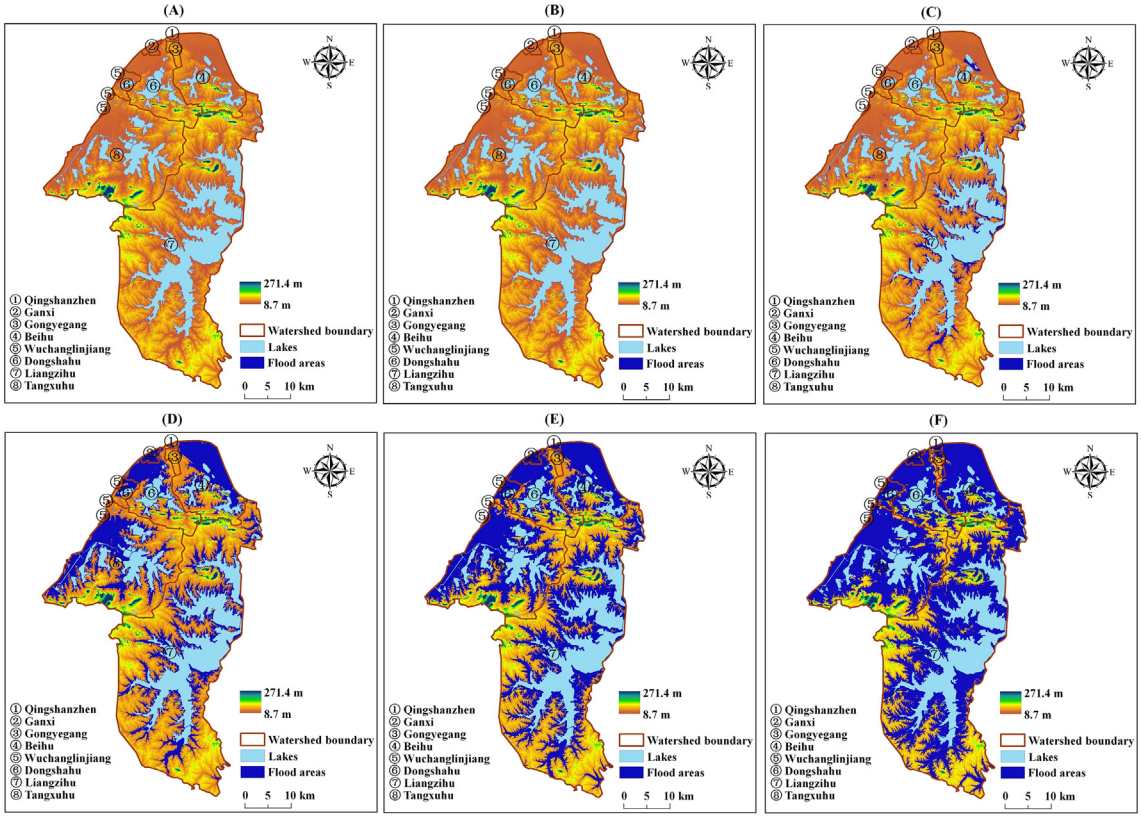

Fig. 8. Urban inundated area map with multi-level watersheds; (A) the water level is 0 m; (B) the water level is 5 m; (C) the water level is 10 m; (D) the water level is 15 m; (E) the water level is 20 m; (F) the water level is 25 m (the water level is calculated relative to the lowest point of DEM).

Table 6
The urban runoff volume in eight administrative watersheds and storage capacity of the dynamic watershed.

Administrative watershed name	Runoff volume (km^3)	Storage capacity(km^3) of 15 m	Storage capacity (km^3) of 20 m
Beihu	39.03×10^{-3}	362.38×10^{-3}	8826.32×10^{-3} (one dynamic watershed)
Dongshahu	56.34×10^{-3}	245.64×10^{-3}(one dynamic watershed)	
Gangxi	4.54×10^{-3}	0.21×10^{-3}	
Gongyegang	7.73×10^{-3}	2384.20×10^{-3}	
Liangzihu	76.25×10^{-3}	1.26×10^{-3}	
Qingshanzhen	1.71×10^{-3}	729.05×10^{-3}	
Tangxunhu	99.51×10^{-3}	0.79×10^{-3}	
Wuchang linjiang	1.73×10^{-3}		

in Fig. 6. IS ratio increased from 3.44% in 1987 to 9.64% in 2002, and runoff volume increased 0.22 km^3 in 1987 to 0.51 km^3 in 2002. Then the IS ratio grew slowly from 9.64% in 2002 to 11.47% in 2012, and runoff volume increased 0.51 km^3 in 1987 to 0.58 km^3 in 2012. The IS ratio accelerated rapidly from 11.47% in 2012 to 16.95% in 2017, and runoff volume increased 0.58 km^3 in 1987 to 0.81 km^3 in 2012. Therefore, impervious surface changes play an important role in urban waterlogging.

4.2.2. Administrative watershed level

For twenty-two watersheds, the overall impervious surface ratio is proportional to the runoff. When the proportion of the impervious surface increases, the runoff increases. However, in the 7, 8, 10–14, 16, 19, 22 watershed, especially the 7–8, 10–13, 22 watershed, the impervious surface ratio accounts for > 60% of the watershed area, or even > 90%; the runoff is less than other watersheds because its runoff is not only related to the proportion of the impervious surface but also related to the area. Although the proportion of impervious surface of these watersheds is high, the area is smaller and so the runoff (see Fig. 7).

4.2.3. Dynamic watershed level

A watershed is usually an appropriately sized region calculated according to DEM. The watershed is planned according to the topography of the watershed, the distribution of pipeline networks within the watershed, and the location and capacity of pumping station facilities. It is a relatively scientific management unit for water control, management, and water cycle planning.

The downtown area of Wuhan is divided into twenty-two watersheds, each of which varies in size. This paper selects eight watersheds in the downtown area of Wuhan for illustration. The DEM data has a spatial resolution of 30 m with the lowest elevation point of 8.7 m and the highest elevation point of 271.4 m. Through rain and flood analysis, under normal circumstances, each watershed has a natural small water system with numerous lakes, as shown in Fig. 8(A). When the rainfall occurs, the level of the lakes in the watershed will rise, and multiple natural lakes will merge into one, which may form a larger watershed, as shown in Fig. 8(D). If the rainfall is even greater, multiple watersheds will be connected, as shown in Fig. 8(E&F). Along with the continuous process of rainfall, managing risk requires dynamic, scientific, and auxiliary decision making based on a multi-scale monitoring model.

Fig. 8(A) shows the urban inundated area map. When the rainfall occurs, the level of the lakes in the watershed will rise, multiple natural lakes will be merged into one larger watershed, as shown in Fig. 8(D), and Gangxi watershed and Dongshahu watershed were merged into one watershed when the water level is 15 m, the storage capacity is 245.64×10^{-3} km^3. The second column in Table 6 shows the urban runoff volume in eight administrative watersheds, and the third column is the storage capacity of the dynamic watershed according to the location of Fig. 8(D). If the rainfall is even greater, as shown in Fig. 8(E), all the eight administrative watersheds are merged into one dynamic

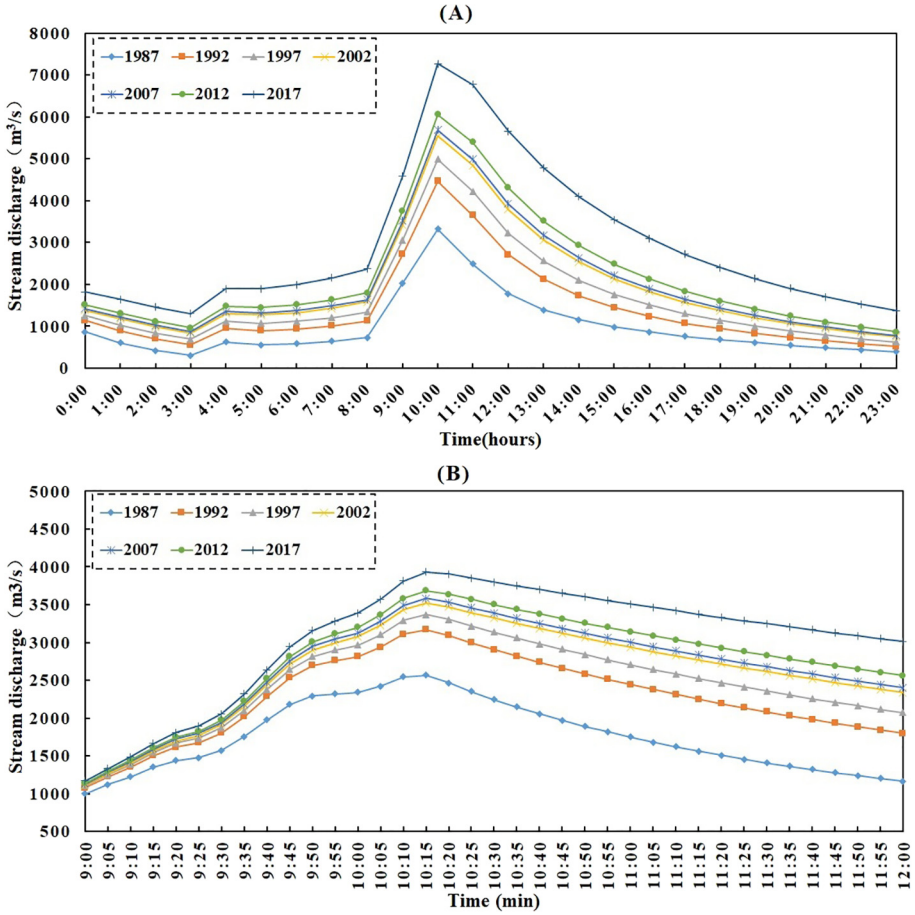

Fig. 9. Hydrographs of area with different imperviousness.

watershed, and the storage capacity is 8826.32 × 10^{-3} km^3 when the water level is 20 m in the fourth column in Table 6.

4.3. The continuous runoff process at different urbanization degrees under the same precipitation event

In order to reflect the continuous runoff process at different urbanization levels under the same precipitation event, the hourly and 5 min precipitation data of July 7, 2013 are used to simulate the hydrograph of the impervious surface ratio in seven different periods in Wuhan from 1987 to 2017. When the ratio of the impervious surface is 4%, the hydrograph is a relatively gentle curve. As the proportion of the impervious surface increases, the curve begins to steepen, and there is a steep ascent and descent process (Fig. 9). When the impervious surface ratio reaches 20%, the discharge is more than twice as large as that when the impervious surface ratio of 4%. At the same time, from 9:00 to 12:00, there is a sharp increase and then a decline due to the increase in rainfall. The hydrograph is simulated every 5 min between 9:00 and 12:00. When the ratio of the impervious surface reaches 20%, the discharge is more than twice that when impervious ratio is 4%. This suggests that under the same drainage system, it is necessary to discharge more water in a shorter period of time. The amount of water entering the lower reaches of the river basin is bound to change in size and duration and touch the peak of the flood much earlier. A higher degree of urbanization leads to a steeper curve as well as greater changes in the total runoff.

5. Discussion

5.1. Analysis of urban impervious monitoring unit on hydrological environmental application

Land use planning, at the city level, regional level, or community level, usually uses the traditional administrative boundaries. From the perspective of urban water cycles, this is unscientific. In urban management, administrative boundary is also used as the basic unit. Previous studies mostly focused on small areas of field analysis, and simulated total runoff volume and peak runoff reduction of implemented LID technology with SWMM modeling or Info Works Model (Ahiablame et al., 2012; Cipolla et al., 2016; Ghimire et al., 2014; Palla et al., 2017). Only few studies analyzed the suitable implementation locations of LID at city or community scale (Song and Chung, 2017). In addition, there is a lack of urban multi-level watershed runoff monitoring to provide the integrated decision-support information for urban flooding management strategies. In 2015, China launched the National Strategy for the Construction of Sponge Cities. The department in charge, the Ministry of Housing and Urban-Rural Development of China, has selected 30 cities as pilot cities in China in two batches. But at presents, each pilot city selected communities or parks no > 100 km^2 as the sponge city reconstruction area, which are not the most scientific solution, because these communities or parks belong to administrative boundaries. Watersheds are suggested to be the better units in a wide spectrum in hydrology field ranging from management to engineering design. The results from 4.2 to 4.4 show that the research on the relationship between impervious surfaces and urban runoffs at multi-scale watersheds is more scientific for hydrological environmental applications.

5.2. Urban hydrological modeling needs DEM information with higher accuracy than DEM products used by the government

Models developed to simulate storm water flows from urban areas differ from models developed to estimate flows in rural areas. Models of urban areas are generally more complicated because additional factors such as gutters, streets, sewers, overflows, and surcharging, closed conduits under pressure, storm water drainage networks, culverts, open channels, roof top storage, open and natural watercourses, and storages may be involved.

More importantly, urban hydrological modeling needs more accurate DEM information than current DEM products used by decision-makers. Raster image data need to be registered to a specific watershed scale, rather than the whole city, for urban hydrological modeling. As many cities are built at flat terrain areas, accurate DEM is needed for detailed multi-scale monitoring. Moreover, the watersheds of a city cannot be analyzed in isolation, as urban rain flood is a dynamic process. With the rise of water level, the submerged area will change, and multiple water systems can be integrated and merged into a larger new watershed.

6. Conclusion

This paper demonstrates that GEE provides a convenient platform for spatial-temporal dynamics analysis. The results show the pervious surfaces can act as an efficient indicator to evaluate and monitor the urban hydrological environment. The increased distribution of pervious surfaces will notably reduce the risk of urban flooding. Similar assessments would be valuable to gain insight into this need for maintenance, which should be kept in mind in the planning of sponge cities to definitely ensure their long-term sustainability.

This paper put forward an urban multi-level watersheds runoff monitoring model, which can be used to analyze the relationship between impervious surfaces and urban runoffs at multi-scale watersheds. In this study, the INFOWORKS model was used to analyze runoffs at multi-level watersheds. The pilot practices in Wuhan showed urban runoff mitigation at watershed scale under different levels. Revision of the existing urban planning and reconstruction will provide significant opportunities to explore critical aspects of environmental sustainability ecologically.

At present, the most powerful dataset is multi-temporal Landsat data shared by GEE or USGS. With the deepening demand for global urban environmental applications, sharing high-resolution remote sensing images is the trend. Further research includes extracting impervious surfaces of higher accuracy at multiple scales from high-resolution time series remote sensing images, which will act as water monitoring parameters for urban planning.

Acknowledgements

This work was supported in part by the National Key Research and Development of China on strategic international scientific and technological innovation cooperation special project under Grant 2016YFE0202300, the National Natural Science Foundation of China under Grants 61671332, 41771452, 51708426, 41890820 and 41771454, the Natural Science Foundation of Hubei Province in China under Grant 2018CFA007, the Independent Research Projects of Wuhan University under Grant 2042018kf0250.

References

Ahiablame, L.M., Engel, B.A., Chaubey, I., 2012. Effectiveness of low impact development practices: literature review and suggestions for future research. Water Air Soil Pollut. 223, 4253–4273. https://doi.org/10.1007/s11270-012-1189-2.

Brabec, E., Schulte, S., Richards, P.L., 2002. Impervious surfaces and water quality: a review of current literature and its implications for watershed planning impervious surfaces and water quality: a review of current literature and its implications. J. Plan. Lit. 16, 499–514.

Breiman, L., 1996. Bagging predictors - Springer. Mach. Learn. 140, 123–140. https://doi.org/10.1007/BF00058655.

Breiman, L., 2001. Random forests. Mach. Learn. 45, 5–32. https://doi.org/10.1023/A:1010933404324.

Brun, S.E., Band, L.E., 2000. Simulating runoff behavior in an urbanizing watershed. Comput. Environ. Urban. Syst. 24, 5–22. https://doi.org/10.1016/S0198-9715(99)00040-X.

Cembrano, G., Quevedo, J., Salamero, M., Puig, V., Figueras, J., Mart, J., 2004. Optimal control of urban drainage systems. A case study. Control. Eng. Pract. 12, 1–9. https://doi.org/10.1111/j.1532-5415.1983.tb05098.x.

Chan, F.K.S., Griffiths, J.A., Higgitt, D., Xu, S., Zhu, F., Tang, Y.T., Xu, Y., Thorne, C.R., 2018. "Sponge City" in China—a breakthrough of planning and flood risk management in the urban context. Land Use Policy 76, 772–778. https://doi.org/10.1016/j.landusepol.2018.03.005.

Chen, B., Xiao, X., Li, X., Pan, L., Doughty, R., Ma, J., Dong, J., Qin, Y., Zhao, B., Wu, Z., Sun, R., Lan, G., Xie, G., Clinton, N., Giri, C., 2017. A mangrove forest map of China in 2015: analysis of time series Landsat 7/8 and Sentinel-1A imagery in Google Earth Engine cloud computing platform. ISPRS J. Photogramm. Remote Sens. 131, 104–120. https://doi.org/10.1016/j.isprsjprs.2017.07.011.

Cipolla, S.S., Maglionico, M., Stojkov, I., 2016. A long-term hydrological modelling of an extensive green roof by means of SWMM. Ecol. Eng. 95, 876–887. https://doi.org/10.1016/j.ecoleng.2016.07.009.

Crippen, R.E., 1990. Calculating the vegetation index faster. Remote Sens. Environ. 34, 71–73. https://doi.org/10.1016/0034-4257(90)90085-z.

Deng, C., Wu, C., 2012. BCI: a biophysical composition index for remote sensing of urban environments. Remote Sens. Environ. 127, 247–259. https://doi.org/10.1016/j.rse.2012.09.009.

Deng, C., Wu, C., 2013a. A spatially adaptive spectral mixture analysis for mapping subpixel urban impervious surface distribution. Remote Sens. Environ. 133, 62–70. https://doi.org/10.1016/j.rse.2013.02.005.

Deng, C., Wu, C., 2013b. The use of single-date MODIS imagery for estimating large-scale urban impervious surface fraction with spectral mixture analysis and machine learning techniques. ISPRS J. Photogramm. Remote Sens. 86, 100–110. https://doi.org/10.1016/j.isprsjprs.2013.09.010.

Deng, C., Li, C., Zhu, Z., Lin, W., Xi, L., 2017. Evaluating the impacts of atmospheric correction, seasonality, environmental settings, and multi-temporal images on sub-pixel urban impervious surface area mapping with Landsat data. ISPRS J. Photogramm. Remote Sens. 133, 89–103. https://doi.org/10.1016/j.isprsjprs.2017.09.015.

Ding, J., Cai, J., Guo, G., Chen, C., 2018. An emergency decision-making method for urban rainstorm water-logging: a China study. Sustainability 10, 3453. https://doi.org/10.3390/su10103453.

Dong, J., Xiao, X., Menarguez, M.A., Zhang, G., Qin, Y., Thau, D., Biradar, C., Moore, B., 2016. Mapping paddy rice planting area in northeastern Asia with Landsat 8 images, phenology-based algorithm and Google Earth Engine. Remote Sens. Environ. 185, 142–154. https://doi.org/10.1016/j.rse.2016.02.016.

Du, P., Liu, S., Liu, P., Tan, K., Cheng, L., 2014. Sub-pixel change detection for urban land-cover analysis via multi-temporal remote sensing images. Geo-Spatial Inf. Sci. 17, 26–38. https://doi.org/10.1080/10095020.2014.889268.

Ghimire, S.R., Johnston, J.M., Ingwersen, W.W., Hawkins, T.R., 2014. Life cycle assessment of domestic and agricultural rainwater harvesting systems. Environ. Sci. Technol. 48, 4069–4077. https://doi.org/10.1021/es500189f.

Goetz, S.J., Wright, R.K., Smith, A.J., Zinecker, E., Schaub, E., 2003. IKONOS imagery for resource management: tree cover, impervious surfaces, and riparian buffer analyses in the mid-Atlantic region. Remote Sens. Environ. 88, 195–208. https://doi.org/10.1016/j.rse.2003.07.010.

Gorelick, N., Hancher, M., Dixon, M., Ilyushchenko, S., Thau, D., Moore, R., 2017. Google Earth Engine: planetary-scale geospatial analysis for everyone. Remote Sens. Environ. 202, 18–27. https://doi.org/10.1016/j.rse.2017.06.031.

Holman-Dodds, J.K., Bradley, A.A., Potter, K.W., 2003. Evaluation of hydrologic benefits of infiltration based urban storm water management. J. Am. Water Resour. Assoc. 39, 205–215.

Horton, R.E., 1933. The role of infiltration in the hydrologic cycle. Trans. Am. Geophys. Union (1), 446–460.

Hu, M., Sayama, T., Zhang, X., Tanaka, K., Takara, K., Yang, H., 2017. Evaluation of low impact development approach for mitigating flood inundation at a watershed scale in China. J. Environ. Manage. 193, 430–438. https://doi.org/10.1016/j.jenvman.2017.02.020.

Huang, H., Chen, Y., Clinton, N., Wang, J., Wang, X., Liu, C., Gong, P., Yang, J., Bai, Y., Zheng, Y., Zhu, Z., 2017. Mapping major land cover dynamics in Beijing using all Landsat images in Google Earth Engine. Remote Sens. Environ. 202, 166–176. https://doi.org/10.1016/j.rse.2017.02.021.

Huete, A.R., 1988. A soil-adjusted vegetation index (SAVI). Remote Sens. Environ. 25, 295–309. https://doi.org/10.1016/0034-4257(88)90106-x.

Im, J., Lu, Z., Rhee, J., Quackenbush, L.J., 2012. Impervious surface quantification using a synthesis of artificial immune networks and decision/regression trees from multi-sensor data. Remote Sens. Environ. 117, 102–113. https://doi.org/10.1016/j.rse.2011.06.024.

Johansen, K., Phinn, S., Taylor, M., 2015. Mapping woody vegetation clearing in Queensland, Australia from Landsat imagery using the Google Earth Engine. Remote Sens. Appl. Soc. Environ. 1, 36–49. https://doi.org/10.1016/j.rsase.2015.06.002.

Jun, L., Fuling, B., 2000. 4D data fusion technique in urban waterlog-draining decision support system. Geo-Spatial Inf. Sci. 3, 42–46. https://doi.org/10.1007/BF02826608.

Kong, F., Ban, Y., Yin, H., James, P., Dronova, I., 2017. Modeling stormwater

management at the city district level in response to changes in land use and low impact development. Environ. Model. Softw. 95, 132–142. https://doi.org/10.1016/j.envsoft.2017.06.021.

Kuang, W., Liu, J., Zhang, Z., Lu, D., Xiang, B., 2013. Spatiotemporal dynamics of impervious surface areas across China during the early 21st century. Chin. Sci. Bull. 58, 1691–1701. https://doi.org/10.1007/s11434-012-5568-2.

Lee, J.S.H., Wich, S., Widayati, A., Koh, L.P., 2016. Detecting industrial oil palm plantations on Landsat images with Google Earth Engine. Remote Sens. Appl. Soc. Environ. 4, 219–224. https://doi.org/10.1016/j.rsase.2016.11.003.

Leopold, L.B., 1968. Hydrology for Urban Land Planning - a Guidebook on the Hydrologic Effects of Urban Land Use.

Li, D., Ma, J., Cheng, T., van Genderen, J.L., Shao, Z., 2018. Challenges and opportunities for the development of MEGACITIES. Int. J. Digit. Earth 0, 1–14. https://doi.org/10.1080/17538947.2018.1512662.

Liu, C., Shao, Z., Chen, M., Luo, H., 2014. MNDISI: a multi- source composition index for impervious surface area estimation at the individual city scale. Remote Sens. Lett. 5, 204. https://doi.org/10.1080/2150704X.2014.895586.

Liu, H., Jia, Y., Niu, C., 2017. “Sponge city” concept helps solve China's urban water problems. Environ. Earth Sci. 76, 473. https://doi.org/10.1007/s12665-017-6652-3.

Liu, X., Hu, G., Chen, Y., Li, X., Xu, X., Li, S., Pei, F., Wang, S., 2018. High-resolution multi-temporal mapping of global urban land using Landsat images based on the Google Earth Engine platform. Remote Sens. Environ. 209, 227–239. https://doi.org/10.1016/j.rse.2018.02.055.

Lu, D., Weng, Q., 2006. Use of impervious surface in urban land-use classification. Remote Sens. Environ. 102, 146–160. https://doi.org/10.1016/j.rse.2006.02.010.

Lu, D., Li, G., Moran, E., Batistella, M., Freitas, C.C., 2011. Mapping impervious surfaces with the integrated use of Landsat thematic mapper and radar data: a case study in an urban-rural landscape in the Brazilian Amazon. ISPRS J. Photogramm. Remote Sens. 66, 798–808. https://doi.org/10.1016/j.isprsjprs.2011.08.004.

McFeeters, S.K., 1996. The use of the Normalized Difference Water Index (NDWI) in the delineation of open water features. Int. J. Remote Sens. 17, 1425–1432. https://doi.org/10.1080/01431169608948714.

Mei, C., Liu, J., Wang, H., Yang, Z., Ding, X., Shao, W., 2018. Integrated assessments of green infrastructure for flood mitigation to support robust decision-making for sponge city construction in an urbanized watershed. Sci. Total Environ. 639, 1394–1407. https://doi.org/10.1016/j.scitotenv.2018.05.199.

Miller, J.D., Hess, T., 2017. Urbanisation impacts on storm runoff along a rural-urban gradient. J. Hydrol. 552, 474–489. https://doi.org/10.1016/j.jhydrol.2017.06.025.

Moscrip, A.L., Montgomery, D.R., 1997. Urbanization, flood frequency, and salmon abundance in Puget lowland streams. J. Am. Water Resour. Assoc. 33, 1289–1297. https://doi.org/10.1111/j.1752-1688.1997.tb03553.x.

Palla, A., Gnecco, I., 2015. Hydrologic modeling of Low Impact Development systems at the urban catchment scale. J. Hydrol. 528, 361–368. https://doi.org/10.1016/j.jhydrol.2015.06.050.

Palla, A., Gnecco, I., La Barbera, P., 2017. The impact of domestic rainwater harvesting systems in storm water runoff mitigation at the urban block scale. J. Environ. Manag. 191, 297–305. https://doi.org/10.1016/j.jenvman.2017.01.025.

Patela, N.N., Angiuli, E., Gamba, P., Gaughan, A., Lisini, G., Stevens, F.R., Tatem, A.J., Trianni, G., 2015. Multitemporal settlement and population mapping from Landsat using google earth engine. Int. J. Appl. Earth Obs. Geoinf. 35, 199–208. https://doi.org/10.1016/j.jag.2014.09.005.

Roodsari, B.K., Chandler, D.G., 2017. Distribution of surface imperviousness in small urban catchments predicts runoff peak flows and stream flashiness. Hydrol. Process. 31, 2990–3002. https://doi.org/10.1002/hyp.11230.

Rosenberg, E.A., Keys, P.W., Booth, D.B., Hartley, D., Burkey, J., Steinemann, A.C., Lettenmaier, D.P., 2010. Precipitation extremes and the impacts of climate change on stormwater infrastructure in Washington State. Clim. Chang. 102, 319–349. https://doi.org/10.1007/s10584-010-9847-0.

Rouse, J.., Haas, R.H., Scheel, J.A., Deering, D.., 1973. Volume I: technical presentations section a. In: Proceedings, 3rd Earth Resource Technology Satellite (ERTS) Symposium, pp. 48–62.

Shao, W., Zhang, H., Liu, J., Yang, G., Chen, X., Yang, Z., Huang, H., 2016. Data integration and its application in the Sponge City construction of China. Procedia Eng 154, 779–786. https://doi.org/10.1016/j.proeng.2016.07.583.

Song, J.Y., Chung, E.S., 2017. A multi-criteria decision analysis system for prioritizing sites and types of low impact development practices: case of Korea. Water (Switzerland) 9. https://doi.org/10.3390/w9040291.

Sunde, M., He, H.S., Hubbart, J.A., Scroggins, C., 2016. Forecasting streamflow response to increased imperviousness in an urbanizing Midwestern watershed using a coupled modeling approach. Appl. Geogr. 72, 14–25. https://doi.org/10.1016/j.apgeog.2016.05.002.

U.S Environmental Protection Agency (USEPA), 2000. Low Impact Development (LID) A Literature Review. U.S Environmental Protection Agency, Washington, D.C.

Wang, Y., Sun, M., Song, B., 2017. Public perceptions of and willingness to pay for sponge city initiatives in China. Resour. Conserv. Recycl. 122, 11–20. https://doi.org/10.1016/j.resconrec.2017.02.002.

Wu, C., Murray, A.T., 2003. Estimating impervious surface distribution by spectral mixture analysis. Remote Sens. Environ. 84, 493–505. https://doi.org/10.1016/S0034-4257(02)00136-0.

Xian, G., Homer, C., 2010. Remote sensing of environment updating the 2001 National Land Cover Database Impervious Surface Products to 2006 using Landsat imagery change detection methods. Remote Sens. Environ. 114, 1676–1686. https://doi.org/10.1016/j.rse.2010.02.018.

Xiong, J., Thenkabail, P.S., Gumma, M.K., Teluguntla, P., Poehnelt, J., Congalton, R.G., Yadav, K., Thau, D., 2017. Automated cropland mapping of continental Africa using Google Earth Engine cloud computing. ISPRS J. Photogramm. Remote Sens. 126, 225–244. https://doi.org/10.1016/j.isprsjprs.2017.01.019.

Xu, Y.S., Shen, S.L., Lai, Y., Zhou, A.N., 2018. Design of sponge city: lessons learnt from an ancient drainage system in Ganzhou, China. J. Hydrol. 563, 900–908. https://doi.org/10.1016/j.jhydrol.2018.06.075.

Xue, F., Huang, M., Wang, W., Zou, L., 2016. Numerical simulation of urban waterlogging based on flood area model. Adv. Meteorol. 2016. https://doi.org/10.1155/2016/3940707.

Yao, L., Chen, L., Wei, W., 2016. Assessing the effectiveness of imperviousness on stormwater runoff in micro urban catchments by model simulation. Hydrol. Process. 30, 1836–1848. https://doi.org/10.1002/hyp.10758.

Zha, Y., Gao, J., Ni, S., 2003. Use of normalized difference built-up index in automatically mapping urban areas from TM imagery. Int. J. Remote Sens. 24, 583–594. https://doi.org/10.1080/01431160304987.

Zhang, X., Xiao, P., Feng, X., 2013. Impervious surface extraction from high-resolution satellite image using pixel- and object-based hybrid analysis. Int. J. Remote Sens. 34, 4449–4465. https://doi.org/10.1080/01431161.2013.779044.

Zhang, Y., Zhang, H., Lin, H., 2014. Improving the impervious surface estimation with combined use of optical and SAR remote sensing images. Remote Sens. Environ. 141, 155–167. https://doi.org/10.1016/j.rse.2013.10.028.

Zhang, L., Weng, Q., Shao, Z., 2017. An evaluation of monthly impervious surface dynamics by fusing Landsat and MODIS time series in the Pearl River Delta, China, from 2000 to 2015. Remote Sens. Environ. 201, 99–114. https://doi.org/10.1016/j.rse.2017.08.036.

Zhang, H., Lin, H., Wang, Y., 2018. A new scheme for urban impervious surface classification from SAR images. ISPRS J. Photogramm. Remote Sens. https://doi.org/10.1016/j.isprsjprs.2018.03.007.

Zhuo, L., Shi, Q., Tao, H., Zheng, J., Li, Q., 2018. An improved temporal mixture analysis unmixing method for estimating impervious surface area based on MODIS and DMSP-OLS data. ISPRS J. Photogramm. Remote Sens. 142, 64–77. https://doi.org/10.1016/j.isprsjprs.2018.05.016.